Thermo-hydro-mechanical coupled modelling of frost actions in unsaturated soils

Emad Norouzi, Biao Li
Department of Building, Civil and Environmental Engineering, Concordia University, Montreal, Quebec, Canada
Hong-Hu Zhu
School of Earth Science and Engineering, Nanjing University, Nanjing, China

GeoCalgary 2022 October 2-5 Reflection on Resources

ABSTRACT
An accurate prediction of frost actions in unsaturated frozen soil is crucial for engineering projects in cold regions. Compared with frost actions in saturated soil, more physical variables, such as the air flux, vapor-water phase change should be incorporated to predict the frost heave in unsaturated soil. The effects of vapor, dry air on frost actions in unsaturated frozen soils have not been systematically analyzed in the literature due to the complexity of multi-physics processes. This paper presents a novel finite element model for simulating fully coupled thermo-hydro-mechanical processes in partially saturated soils exposed to freeze-thaw cycles. Physical processes include linear momentum conservation, heat conduction and convection, water-ice phase change, water (moisture) movement through cryo-suction, airflow, and the development of independent ice lenses. The water-ice phase change is modelled by means of a non-equilibrium approach considering both water supercooling and a hysteresis of ice content. The coupled nonlinear partial differential equations are solved numerically by means of the finite element method (FEM) using our in-house developed numerical code. The numerical results on frost actions of a seasonal frozen soil are demonstrated using our numerical code.

RÉSUMÉ
Une prédiction précise des actions du gel dans un sol gelé non saturé est cruciale pour les projets d'ingénierie dans les régions froides. Par rapport aux actions du gel dans un sol saturé, des variables plus physiques, telles que le flux d'air, le changement de phase vapeur-eau doivent être incorporées pour prédire le soulèvement par le gel dans un sol non saturé. Les effets de la vapeur et de l'air sec sur les actions du gel dans les sols gelés non saturés n'ont pas été systématiquement analysés dans la littérature en raison de la complexité des processus multi-physiques. Cet article présente un nouveau modèle d'éléments finis pour simuler des processus thermo-hydro-mécaniques entièrement couplés dans des sols partiellement saturés exposés à des cycles de gel-dégel. Les processus physiques comprennent la conservation de l'impulsion linéaire, la conduction et la convection de la chaleur, le changement de phase eau-glace, le mouvement de l'eau (humidité) par cryo-aspiration, le flux d'air et le développement de lentilles de glace indépendantes. Le changement de phase eau-glace est modélisé au moyen d'une approche de non-équilibre considérant à la fois la surfusion de l'eau et une hystérésis de la teneur en glace. Les équations aux dérivées partielles non linéaires couplées sont résolues numériquement au moyen de la méthode des éléments finis (FEM) en utilisant notre code numérique développé en interne. Les résultats numériques sur les actions du gel d'un sol gelé de façon saisonnière sont démontrés à l'aide de notre code numérique.

1 INTRODUCTION

Unsaturated frozen soil comprised of soil particles, ice, water, and air is found in the seasonal frozen, artificially frozen, and permafrost layers. The North and South hemispheres such as Siberia, Canada, Greenland, Antarctica, and Alaska are the probable regions that experience the prolonged freezing temperatures (Kadivar and Manahiloh, 2019). Recently, constructions in these regions such as natural foundations, highways, and railways as well as vast application of artificial ground freezing (AGF) in mining and tunneling engineering have been increased (Xu et al., 2019). As an example, approximately 45000 people are living in arctic and subarctic regions in north of Quebec. Also, nearly 10% of earth's surface is covered by collapsible silt-sized loess soils which experience cycling freezing and thawing (Wang et al., 2016).

The permafrost layer consists of unconsolidated sediments, and the contact between the permafrost layer and the bedrock is minimal. Any construction on this sediment creates a large settlement due to the consolidation behavior (Delage et al., 2000). On the other hand, thawing turns the frozen soil into water and soil, and draining water from the medium increases the consolidation rate and reduces the mechanical stiffness of the system. Simultaneous consolidation and stiffness reduction induced cause damages to the structures during and after the construction. The aforementioned ground deformations cause a set of Geo-Risks (e.g., infrastructure damages, subsidence, borehole failures). Including the prediction of mechanical behaviors and reactions of soil to freeze and thawing in construction projects during the

design and build procedure alleviates the negative consequences of Geo-Risks. Reliable model development may reduce the technical damages and has financial and social benefits in the long term. Figure 1 schematically display a soil sample of unsaturated frozen and its mass and volume ratios.

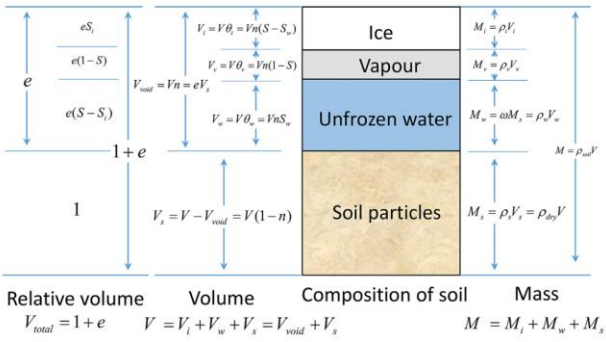

Fig 1. Mass and volume ratios of four-phase composition of an unsaturated frozen soil sample (Huang and Rudolph, 2021).

Several types of research have been conducted to investigate physical-mechanical properties of frozen soil. A series of triaxial compression tests on ice-saturated frozen soil has been carried out under different confining pressures to study various type of the mechanical properties of the frozen soils with different freeze-thaw process (Wang et al. 2017; Zhou et al. 2018a). Accordingly, Zhao and his colleagues derived a linear model to obtain the elastic modulus of frozen saturated clay based on uniaxial compression strength tests at different gradients of temperature and concluded that the elastic modulus decreases with increasing the temperature gradient and average temperature (Zhao et al., 2009). Also, the methods for obtaining the tensile strength, can be generally classified into direct and indirect methods (Ming et al., 2017). In the direct methods, the experiments are usually performed on dumbbell samples which are hard to prepare (Christ and Park 2010). The difficulties of conducting the direct methods lead to perform other methods to estimate the tensile strength indirectly like four point bending test and the Brazilian test (Azmatch et al. 2011; Zhou et al. 2015).

In conjunction with the experimental researches, mathematical and theoretical analysis have been developed to address the constitutive relation of frozen soil (Xu et al. 2011). Yang et al. (2014) characterize the mechanical properties of the artificial frozen silt by performing triaxial compression and creep tests at the temperature of -8^{o}C and presented the relation between the confining pressures and strain softening in shear process. They also developed a constitutive model and compared their model with the tests data. Finally, Li *et al.* (2016a, 2016b) presented a constitutive law based on the empirical functions on long-term elasto-plastic behavior of soil and implemented it on a model framed in Finite Element Method (FEM) and verified their model with the triaxial test data.

Several researches have studied the complex behavior of freeze-thaw action including phase transition, micro-cryo-suction, and theory of premelting dynamics by utilizing the analytical, experimental, and numerical approaches (Kruschwitz and Bluhm 2005). Nishimura et al. derived the formulation and numerical application of fully coupled THM analysis of elasto-plastic water-saturated frozen soils that includes freezing and thawing process by involving the concept of the cryo-suction and concluded that the strength and the stiffness of the frozen soil increases by increasing the cryogenic suction (Nishimura et al., 2009). Cryo-suction is similar to the suction that happens between gas and water in unsaturated unfrozen soil (Shastri and Sanchez, 2012). Also, Zhou and Meschke proposed a three-phases model framed in FEM and considered the theory of premelting dynamics (Zhou and Meschke 2013)

Based on the theory of premelting dynamics, under freezing point temperature, two forms of unfrozen water can be found as supercooled pore water pressure and Interfacial premelting unfrozen film water (Figure 2).

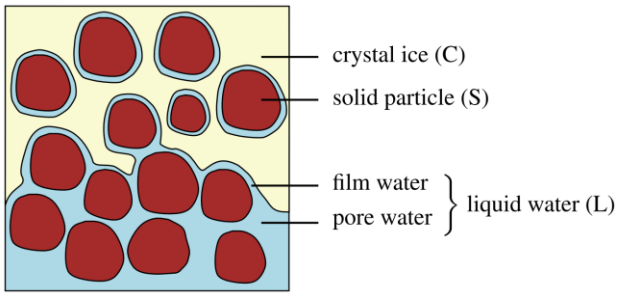

Fig 2. Illustration of the frozen fringe of a frost-susceptible soil (Zhou and Meschke, 2013).

Basically, modelling of the freezing and thawing phenomena including temperature variation, phase change, water and vapor movement, and displacement are studied in the concept of mechanics of porous media. The interactions between parameters due to freezing and thawing can be recognized through developing a set of fully coupled thermo-hyrdro-mechanical (THM) equations.

In particular, numerical modelling of the behavior of unsaturated frozen porous media under freezing and thawing and phase change has been studied recently from different point of view. A fully coupled THM model for variably saturated freezing soil is presented by Huang and Rudolph, (2021) and verified by experimental data. Also, introducing effective strain ratio, Bai et al., (2020) proposed a coupled heat-water-mechanics model to examine the frost heave of saturated and unsaturated soils. However, most of the previous studies cannot comprehensively consider the moisture flow, vapor distribution, phase change, and the deformation of the medium (Gawin et al., 2019). Recently, the deformation of the unsaturated frozen porous media is also included in the numerical models. Gawin et al., (2020) developed a two-dimensional plane strain numerical simulation based on their novel hygro-thermo-mechanical mathematical equations to model sample of concrete under freezing and thawing. In order to consider the effect of ice pressure during freezing process, they have used crystal pressure function. However, the study by Gawin et al. (2020) was only applied to concrete and not yet applicable to soils so far.

In this paper, a two-dimensional fully coupled model is developed to study the mechanical frost action of an

unsaturated frozen soil sample under cycling freezing and thawing scenario.

After introduction, volumetric relations and governing equations such as linear momentum balance, mass balance, and energy balance equations of THM model are introduced in section 2. The auxiliary relations are in section 3. In section 4, the description of numerical simulation and results are provided. Finally, conclusions are in section 5.

2 GOVERNING EQUATIONS

In this section, the volumetric relations and the governing equations of unsaturated frozen porous media are briefly introduced. The details of the equations as well as the assumption can be found in references (e.g. Gawin et al., 2020, 2019; Lewis et al., 1998; Norouzi et al., 2019).

2.1 Volumetric Relations

The volume ratio of each phase can be defined as:

$$n_\alpha = \frac{V_\alpha}{V} \quad (\alpha \in s, w, ice, g) \qquad [1]$$

in which V_α is the volume ratio of α phase, V is the total volume, and *s*, *w*, *ice* and *g* are representing soil, water, ice, and moist air respectively. Also, water, ice, and moist air saturation can be defined as:

$$S_k = \frac{V_k}{V_{void}} = \frac{V_k}{V - V_s} \quad (k \in w, ice, g) \qquad [2]$$

and we have:

$$S_w + S_{ice} + S_g = 1 \qquad [3]$$

Also, the effective density of the medium is defined as:

$$\rho_{eff} = (1-n)\rho_s + nS_w\rho_w + +nS_{ice}\rho_{ice} \qquad [4]$$

where ρ_s, ρ_w, and ρ_i are the densities of the solid, water, and ice, respectively.

2.2 Linear Momentum balance Equation

The conservation of linear momentum equation of the porous media is:

$$\nabla.\boldsymbol{\sigma} + \rho\mathbf{b} = 0 \qquad [5]$$

In Equation 5, $\boldsymbol{\sigma}$ is the total stress tensor, "." is the dot product, $\nabla = \langle \partial/\partial x \quad \partial/\partial y \rangle$, and $\mathbf{b}$ is the body force. In this study, a linear elastic isotropic constitutive relation between effective stress and the effective strain is given by:

$$\boldsymbol{\sigma}' = \mathbf{D_c}(\boldsymbol{\varepsilon}_{tot} - \boldsymbol{\varepsilon}^{\mathrm{ph}} - \boldsymbol{\varepsilon}^T) \qquad [6]$$

in which $\boldsymbol{\sigma}'$ is the effective stress tensor, and $\mathbf{D_c}$ is the elastic stiffness matrix. Also, $\boldsymbol{\varepsilon}_{tot}$, $\boldsymbol{\varepsilon}^{\mathrm{ph}}$, and $\boldsymbol{\varepsilon}^T$ are the total strain, the strain due to phase change, and thermal strain, respectively.

According to Bekele et al., (2017) and Gawin et al., (2020), the final form of linear momentum balance equation for the multi-phase material can be written in one of the following forms:

$$\boldsymbol{\sigma} = \boldsymbol{\sigma}' - S_w P^w \mathbf{I} - S_g P^g \mathbf{I} - S_{ice} P^{ice} \mathbf{I} \qquad [7]$$

where P^g, P^w, and P^{ice} are air, water, and ice pressure, and $\mathbf{I}$ is an identity matrix.

2.3 Mass Balance Equation of dry air

The general form of conservation of mass equation for each phase is:

$$\frac{\mathrm{D}}{\mathrm{D}t}(n_\alpha\rho_\alpha) + n_\alpha\rho_\alpha\nabla.v^\alpha - \dot{m}_\alpha = 0 \quad (\alpha \in s, w, ice, g) \qquad [9]$$

In Equation 9, v^α is the velocity of α phase, and $\dot{m}_\alpha$ is the rate of increase or decrease of mass of α phase per volume.

Assuming that moist air is combination of dry air (*ga*) and vapor (*gw*), the moist air pressure can be described as follow:

$$P^g = P^{gw} + P^{ga} \qquad [10]$$

where P^{gw} and P^{ga} are pressure of vapor and dry air, respectively.

Consequently, mass balance equation of dry air can be express as:

$$\begin{aligned} nS_g\frac{\partial\rho^{ga}}{\partial t} + n\rho^{ga}\frac{\partial S_g}{\partial t} + S_g\rho^{ga}\mathrm{div}\overline{\boldsymbol{v}}^s \\ + \mathrm{div}\left[\rho^g\frac{M_aM_w}{{M_g}^2}\mathbf{D}_{gw}\nabla\left(\frac{P^{gw}}{P^g}\right)\right] \\ - \mathrm{div}\left[\rho^{ga}\frac{\mathbf{k}k^{rg}}{\mu^g}(\nabla P^g - \rho^g\mathbf{g})\right] \\ - \beta_{sg}\frac{\partial T}{\partial t} = 0 \end{aligned} \qquad [11]$$

In the above equation, ρ^{ga} is dry air density, M_a, M_w, M_g are molar mass of dry air, water and gas phase, and $\mathbf{D}_{gw}$ is water vapor-dry air diffusivity tensor. Moreover, P^{gw} is the vapor pressure, $\mathbf{u}$ is displacement of medium. Also, $\mathbf{k}$ is intrinsic permeability and $k^{r\alpha}$, and μ^α are relative permeability and viscosity of *α* fluid.

2.4 Mass Balance Equation of water species

Combining the conservation of mass equation of water, ice, and vapor and assuming that the amount of the rate of mass of water and ice are equal with different sign in freezing and thawing conditions (i.e., $\dot{m}_{ice} = -\dot{m}_w$), we have:

$$\begin{aligned} nS_g\frac{\partial\rho^{gw}}{\partial t} + n\rho^{gw}\frac{\partial S_g}{\partial t} + n\rho^w\frac{\partial S_w}{\partial t} + n\rho^{ice}\frac{\partial S_{ice}}{\partial t} \\ - \mathrm{div}\left[\rho^g\frac{M_aM_w}{{M_g}^2}\mathbf{D}_{gw}\nabla\left(\frac{P^{gw}}{P^g}\right)\right] \\ - \mathrm{div}\left[\rho^w\frac{\mathbf{k}k^{rw}}{\mu^w}(\nabla P^w - \rho^w\mathbf{g})\right] \\ - \mathrm{div}\left[\rho^{gw}\frac{\mathbf{k}k^{rg}}{\mu^g}(\nabla P^g - \rho^g\mathbf{g})\right] \\ - \beta_{swg,ice}\frac{\partial T}{\partial t} \\ + \left(S_w\rho^w + S_g\rho^{gw}\right. \\ \left. + S_{ice}\rho^{ice}\right)\mathrm{div}\overline{\boldsymbol{v}}^s = 0 \end{aligned} \qquad [13]$$

in which ρ^{gw} is the density of water vapor. Considering β_w, β_{ice} as water and ice thermal expansion coefficient, $\beta_{swg,ice}$ can be written as follow:

$$\beta_{swg,ice} = (1-n)\left(\rho^{gw}S_g + \rho^{w}S_w\right)\beta_s + n\rho^{w}S_w\beta_w + n\rho^{ice}S_{ice}\beta_{ice} \quad [14]$$

2.5 Energy Balance Equation

It is assumed that all the phases are locally in a state of thermodynamic equilibrium and water vapor mass source caused by the liquid water evaporation – desorption is neglected. Thus, the energy balance equation of the medium can be derived as:

$$\left(\rho C_p\right)_{eff}\frac{\partial T}{\partial t} + \mathbf{a}.\,\mathrm{grad}T + \mathrm{div}\left(\lambda_{eff}\mathrm{grad}T\right) - \dot{m}_{ice/w}\Delta H_{ice,w} = 0 \quad [15]$$

Note that in Equation 9, heat transfer between the phases is neglected. $(\rho C)_{\mathrm{eff}}$ is the effective heat capacity:

$$\left(\rho C_p\right)_{eff} = (1-n)\rho_s C_p^s + nS_w\rho^w C_p^w + nS_g\rho^g C_p^g + nS_{ice}\rho^{ice}C_p^{ice} \quad [16]$$

λ_{eff} is overall thermal conductivity based on Fourier's law and is expressed as:

$$\lambda_{eff} = \lambda_s^{1-n}.\lambda_w^{nS_w}.\lambda_i^{nS_i}.\lambda_g^{nS_g} \quad [17]$$

Also, $\mathbf{a}$ is the vector of advection of heat transfer and is given as:

$$\mathbf{a} = \rho^w C_p^w \mathbf{w}^w + \rho^g C_p^g \mathbf{w}^g \quad [18]$$

Furthermore, $\Delta H_{ice,w}$ is specific enthalpy of water freezing and $\dot{m}_{ice/w}$ is mass source of crystallized water due to liquid pore water freezing (Gawin et al., 2020, 2019)

3 AUXILIARY EQUATIONS

3.1 Equation of State of Perfect Gas

In this study, it is assumed that the moist air in a perfect gas and follows the ideal gas law (Lewis et al., 1998)

$$P^{ga} = \frac{\rho^{ga}TR}{M_a} \quad [19]$$

$$P^{gw} = \frac{\rho^{gw}TR}{M_w} \quad [20]$$

Using above equations, the derivation of dry air and water vapor densities with respect to time can be derived and related to primary variables (i.e. temperature and capillary pressure) as:

$$\begin{aligned}\frac{\partial \rho^{ga}}{\partial t} = \frac{\partial}{\partial t}\left(\frac{P^{ga}M_a}{RT}\right) = \frac{\partial}{\partial t}\left[\frac{(P^g - P^{gw})M_a}{RT}\right] \\ = \frac{M_a}{RT}\frac{\partial P^g}{\partial t} - \frac{M_a P^g}{RT^2}\frac{\partial T}{\partial t} \\ - \frac{M_a}{RT}\frac{\partial P^{gw}}{\partial P^c}\frac{\partial P^c}{\partial t} \\ - \frac{M_a}{RT}\left(\frac{\partial P^{gw}}{\partial T} - \frac{P^{gw}}{T}\right)\frac{\partial T}{\partial t}\end{aligned} \quad [21]$$

$$\begin{aligned}\frac{\partial \rho^{gw}}{\partial t} = \frac{\partial}{\partial t}\left(\frac{P^{gw}M_w}{RT}\right) \\ = \frac{M_w}{RT}\frac{\partial P^{gw}}{\partial P^c}\frac{\partial P^c}{\partial t} \\ + \frac{M_w}{RT}\left(\frac{\partial P^{gw}}{\partial T} - \frac{P^{gw}}{T}\right)\frac{\partial T}{\partial t}\end{aligned} \quad [22]$$

3.2 Relative Humidity

In this paper, relative humidity is defined based on Kelvin-Laplace relation:

$$RH = \frac{P^{gw}}{P_{sat}^{gw}} = \exp\left(-\frac{P^c M_w}{\rho^w RT}\right) \quad [23]$$

in which P_{sat}^{gw} is water vapor saturation pressure that is a function of temperature. Using Equation 19, the derivation of vapor pressure with respect to capillary pressure and temperature can be found as follow:

$$\frac{\partial P^{gw}}{\partial P^c} = -P_{sat}^{gw}\frac{M_w}{\rho^w RT}\exp\left(-\frac{P^c M_w}{\rho^w RT}\right) \quad [24]$$

$$\frac{\partial P^{gw}}{\partial T} = P_{sat}^{gw}\frac{P^c M_w}{\rho^w RT^2}\exp\left(-\frac{P^c M_w}{\rho^w RT}\right) \quad [25]$$

3.3 Soil-Water Characteristic curve

In this paper, in order to relate water saturation to capillary pressure Baroghel-Bounyet et al. 1999 equation is applied:

$$S_w = \left(\left(\frac{P^c}{a}\right)^{\frac{b}{b-1}} + 1\right)^{-\frac{1}{b}} \quad [26]$$

Consequently, the water and gas relative permeability relations are defined as:

$$k^{rw} = \sqrt{S_w}\left(1 - \left(1 - {S_w}^{1/b}\right)^b\right)^2 \quad [27]$$

$$k^{rg} = \sqrt{1-S_w}\left(1 - {S_w}^{1/b}\right)^{2b} \quad [28]$$

where a and b are the experimental parameters. Also, note that it is assumed that because the mass source of crystallized water due to vapor deposition is neglected, the following relation can be established between water and ice saturation:

$$d\left(\rho^{ice}S_{ice}\right) \cong -d(\rho^w S_w) \quad [29]$$

4 NUMERICAL SIMULATION

After introducing the governing and auxiliary equations, the weak forms of governing equations should be derived. By considering the essential and the natural boundary conditions, the discretized set of coupled equations can be rewritten as a nonlinear differential equation in time:

$$\mathbf{K}\mathbf{X} + \mathbf{C}\frac{\partial \mathbf{X}}{\partial t} = \mathbf{F} \quad [30]$$

where $\mathbf{X}^{\mathbf{T}} = [u \quad p^g \quad p^c \quad T]$ is the vector of main variables, $\mathbf{F}$ is the force vector. Also, $\mathbf{K}$ and $\mathbf{C}$ are the coefficients which are the function of the main parameters. Thus, Equation 19 is highly nonlinear. A fully implicit method is utilized to discretized Equation 19 with time, and it is solved by using a Newton-Raphson scheme.

3.4 Model description

In this section, a two-dimensional plane strain sample of unsaturated frozen soil under cycling freezing and thawing is simulated based on aforementioned equations. The model is discretized and solved using Finite Element Method (FEM) in space and Finite Difference Method (FDM) in time. Figure 3 shows the numerical meshing of the sample. Width and height of sample are 10 cm × 40 cm with 16 meshes. Initial temperature and humidity are 8ºC and 97%.

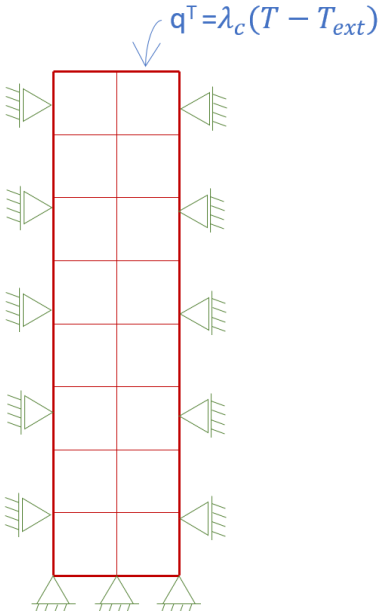

Figure 3. Numerical meshing of plane strain model

The boundary conditions are as follow: At the bottom side, displacement is restricted and water and gas flux are zero and the temperature is constant. At the right and left side, the displacement is restricted at horizontal direction. Also, temperature, gas, and water fluxes are zero. At top side, gas pressure is constant at about 0.1 MPa. Capillary pressure is also constant and heat flux is imposing to change the temperature of the sample. The problem is simulated in 50 hours. In the first 5 hours temperature reduces from 8º C to -12º C. After that for 10 hours external temperature remains constant. Then, it increases to 8º C. After next 5 hours this cycle happens again. Figure 4 depicted the variational of external temperature from initial temperature to final temperature.

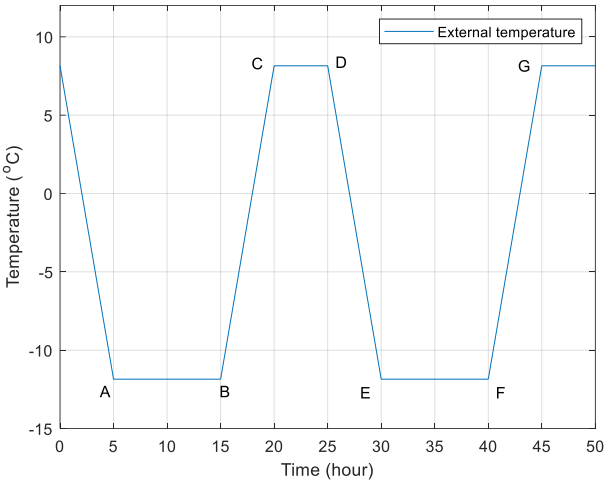

Figure 4. Variation of external temperature versus time.

Material properties of simulation including mechanical, hydraulic and thermal properties of unsaturated soil sample are in Table 1.

Table 1. Model properties of the model

Item	Symbol	Value
Porosity (-)	n	0.122
Density of soil (kg/m^3)	ρ_s	2650
Density of ice (kg/m^3)	ρ_i	910
Density of water (kg/m^3)	ρ_w	1000
Elastic modulus of soil (GPa)	E_s	12
Poisson's ratio of soil (-)	ν_s	0.3
Strength model parameter (-)	η	5
Specific heat capacity of soil (J/kg/K)	C_s	800
Specific heat capacity of ice (J/kg/K)	C_i	4190
Specific heat capacity of water (J/kg/K)	C_w	2095
Thermal conductivity of soil (W/m/K)	λ_s	1.5
Thermal conductivity of ice (W/m/K)	λ_i	0.6
Thermal conductivity of water (W/m/K)	λ_w	2.2
Thermal conductivity of air (W/m/K)	λ_c	1.0
Thermal expansion coefficient (1/K)	β_s	1.24×10^{-5}
Latent heat of fusion (J/kg)	L_f	334000
Water intrinsic permeability (m^2)	$\mathbf{k}$	10^{-19}
Saturation model parameter (Pa^{-1})	a	2×10^6
Saturation model parameter (-)	b	3.0

3.5 Temperature results

Figure 5 shows the contours of temperature at various time. At the initial condition, the temperature is constant at 281 K. As depicted in Figure 5.a after five hours about 30% of the sample is affected that increases to 70% at the end

of the first cycle (Figure 5.d). Also, by comparing Figure 5.b with Figure 5.f, it can be concluded that although the temperature load is the same, the sample is cooler in the second cycle that is because of the heat capacity of the sample. This may cause higher ice saturation and subsidence after each cycle.

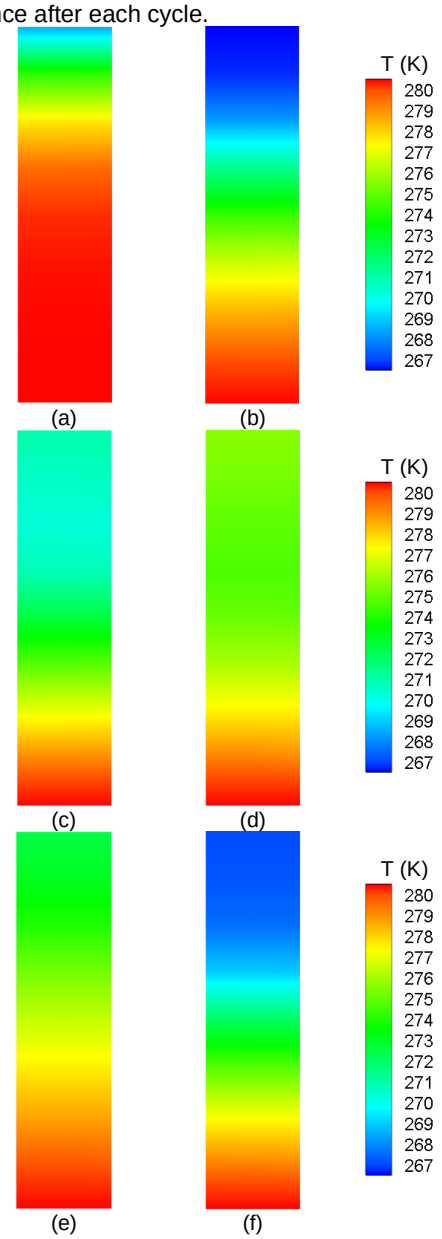

Figure 5. Contours of temperature at (a) 5, (b) 15, (c) 20, (d) 25 (e) 30, and (f) 40 hours.

3.6 Displacement results

Contours of displacement are depicted in Figure 6 at various time. As shown, comparing to first cycle, the maximum amount of deformation reduces at the end of the second cycle. The results also display that the higher subsidence occurs during thawing at the end of first cycle.

In this paper the effect of freezing and thawing on the elastic properties is not considered. Also, for the next cycles soil may experience higher amount of deformation and may extend to plasticity zone. Therefore, providing an unsaturated THM model that considers plasticity behavior seems important.

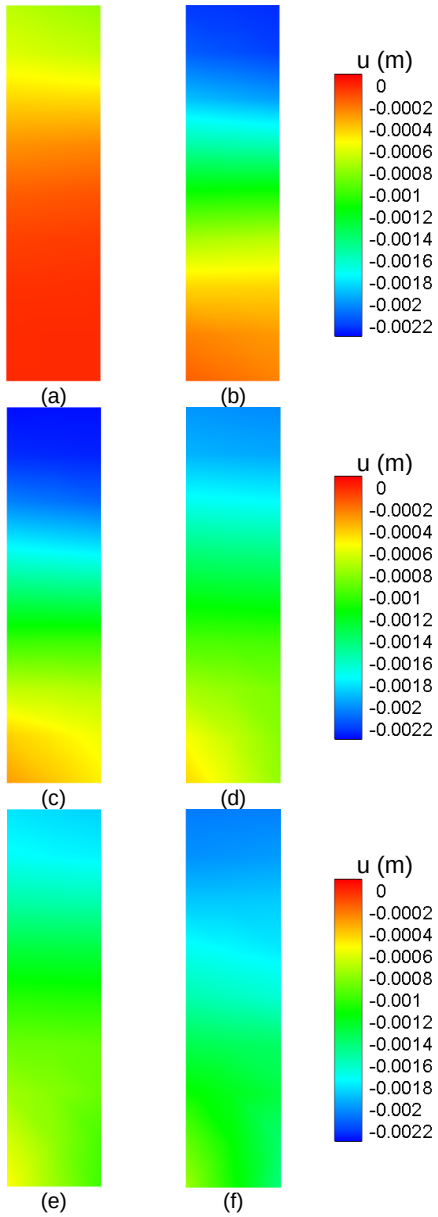

Figure 6. Contours of displacement of sample at (a) 5, (b) 15, (c) 20, (d) 25 (e) 30, and (f) 40 hours.

3.7 Ice saturation results

Results of ice saturation at different height is drawn in Figure 7. The results show that freezing does not happened at the lower level. Furthermore, it is shown that, the rate of freezing and melting in the first cycle is higher than the second one.

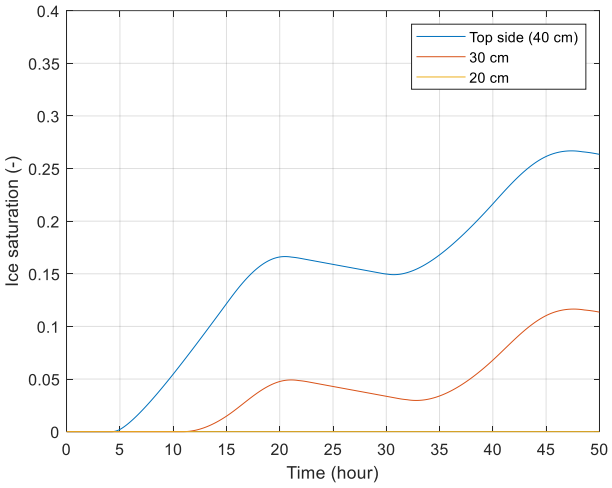

Figure 7. variation of ice saturation versus time.

5 CONCLUSIONS

In this paper a two-dimensional THM model is developed to study the behavior of an unsaturated soil under cycling freezing and thawing. The following results are concluded by studying the variation of different variables such as temperature, ice saturation, and displacement of the sample during the test:

- Based on the derived equation and results, taking the deformation of the model into account will affect the results of key variables, such as gas pressure and ice saturation.
- Cycling freezing and thawing can be considered as an external load which increases at each cycle and extended to bigger part of the model. However, it is shown that the rate of freezing decreases during the second cycle.

6 ACKNOWLEDGMENT

The authors would like to acknowledge the fund provided by NSERC Discovery Grant Canada (NO. RGPIN-2017-05169)

7 REFERENCES

Akagawa, S., Nishisato, K., 2009. Tensile strength of frozen soil in the temperature range of the frozen fringe. Cold Reg. Sci. Technol. 57, 13–22. https://doi.org/https://doi.org/10.1016/j.coldregions.2009.01.002

Azmatch, T.F., Sego, D.C., Arenson, L.U., Biggar, K.W., 2011. Tensile strength and stress–strain behaviour of Devon silt under frozen fringe conditions. Cold Reg. Sci. Technol. 68, 85–90. https://doi.org/https://doi.org/10.1016/j.coldregions.2011.05.002

Azmatch, T.F., Sego, D.C., Arenson, L.U., Biggar, K.W., 2010. Tensile strength of frozen soils using four-point bending test, in: Proceedings of the 63rd Canadian Geotechnical Conference and 6th Canadian Permafrost Conference, Calgary, Canada. pp. 436–442.

Azmatch, T.F., Sego, D.C., Arenson, L.U., Biggar, K.W., 2007. Tensile Strength of Frozen Soils Using Four-Point Bending Test 436–442.

Bai, R., Lai, Y., Pei, W., Zhang, M., 2020. Investigation on frost heave of saturated–unsaturated soils. Acta Geotech. 15, 3295–3306.

Bekele, Y.W., Kyokawa, H., Kvarving, A.M., Kvamsdal, T., Nordal, S., 2017. Isogeometric analysis of THM coupled processes in ground freezing. Comput. Geotech. 88, 129–145.

Christ, M., Park, J.-B., 2010. Laboratory determination of strength properties of frozen rubber–sand mixtures. Cold Reg. Sci. Technol. 60, 169–175. https://doi.org/https://doi.org/10.1016/j.coldregions.2009.08.013

Delage, P., Sultan, N., Cui, Y.J., 2000. On the thermal consolidation of Boom clay. Can. Geotech. J. 37, 343–354.

Gawin, D., Pesavento, F., Koniorczyk, M., Schrefler, B.A., 2020. Poro-mechanical model of strain hysteresis due to cyclic water freezing in partially saturated porous media. Int. J. Solids Struct. 206, 322–339.

Gawin, D., Pesavento, F., Koniorczyk, M., Schrefler, B.A., 2019. Non-equilibrium modeling hysteresis of water freezing: Ice thawing in partially saturated porous building materials. J. Build. Phys. 43, 61–98.

Huang, X., Rudolph, D.L., 2021. Coupled model for water, vapour, heat, stress and strain fields in variably saturated freezing soils. Adv. Water Resour. 154, 103945.

Kadivar, M., Manahiloh, K.N., 2019. Revisiting parameters that dictate the mechanical behavior of frozen soils. Cold Reg. Sci. Technol. 163, 34–43. https://doi.org/https://doi.org/10.1016/j.coldregions.2019.04.005

Kruschwitz, J., Bluhm, J., 2005. Modeling of ice formation in porous solids with regard to the description of frost damage. Comput. Mater. Sci. 32, 407–417.

Lewis, Roland W, Lewis, Roland Wynne, Schrefler, B.A., 1998. The finite element method in the static and dynamic deformation and consolidation of porous media. John Wiley & Sons.

Li, Q., Ling, X., Technology, D.S.-C.R.S. and, 2016, U., 2016a. Elasto-plastic behaviour of frozen soil subjected to long-term low-level repeated loading, Part I: Experimental investigation. Cold Reg. Sci. Technol. 125, 138–151.

Li, Q., Ling, X., Technology, D.S.-C.R.S. and, 2016, U., 2016b. Elasto-plastic behaviour of frozen soil subjected to long-term low-level repeated loading, Part II: Constitutive modelling. Cold Reg. Sci. Technol. 122, 58–70.

Mikkola, M., Hartikainen, J., 2001. Mathematical model of soil freezing and its numerical implementation. Int. J. Numer. Methods Eng. 52, 543–557.

Ming, F., Li, D., Zhang, M., Zhang, Y., 2017. A novel method for estimating the elastic modulus of frozen soil. Cold Reg. Sci. Technol. 141, 1–7. https://doi.org/https://doi.org/10.1016/j.coldregions.2017.05.005

Nishimura, S., Gens, A., Olivella, S., Jardine, R.J., 2009.

Thm-coupled finite element analysis of frozen soil: Formulation and application. Geotechnique 59, 159–171. https://doi.org/10.1680/geot.2009.59.3.159

Norouzi, E., Moslemzadeh, H., Mohammadi, S., 2019. Maximum entropy based finite element analysis of porous media. Front. Struct. Civ. Eng. 13, 364–379.

Razbegin, V.N., Vyalov, S.S., Maksimyak, R. V, Sadovskii, A. V, 1996. Mechanical properties of frozen soils. Soil Mech. Found. Eng. 33, 35–45. https://doi.org/10.1007/BF02354292

Shastri, A., Sanchez, M., 2012. Mechanical Modeling of Frozen Soils Incorporating the Effect of Cryogenic Suction and Temperature 2492–2501. https://doi.org/10.1061/9780784412121.255

Wang, J., Nishimura, S., Tokoro, T., 2017. Laboratory study and interpretation of mechanical behavior of frozen clay through state concept. Soils Found. 57, 194–210. https://doi.org/https://doi.org/10.1016/j.sandf.2017.03.003

Wang, S., Lv, Q., Baaj, H., Li, X., Zhao, Y., 2016. Volume change behaviour and microstructure of stabilized loess under cyclic freeze–thaw conditions. Can. J. Civ. Eng. 43, 865–874.

Xu, X., Lai, Y., Chai, J., Fan, C., 2014. Laboratory investigation on the mechanical behavior of ice-saturated frozen loess. Sci. Cold Arid Reg. 6, 314–321.

Xu, X., Lai, Y., Dong, Y., Qi, J., 2011. Laboratory investigation on strength and deformation characteristics of ice-saturated frozen sandy soil. Cold Reg. Sci. Technol. 69, 98–104. https://doi.org/https://doi.org/10.1016/j.coldregions.2011.07.005

Xu, X., Li, Q., Lai, Y., Pang, W., Zhang, R., 2019. Effect of moisture content on mechanical and damage behavior of frozen loess under triaxial condition along with different confining pressures. Cold Reg. Sci. Technol. 157, 110–118. https://doi.org/https://doi.org/10.1016/j.coldregions.2018.10.004

Yang, Y., Gao, F., Cheng, H., Lai, Y., Zhang, X., 2014. Researches on the Constitutive Models of Artificial Frozen Silt in Underground Engineering. Adv. Mater. Sci. Eng. 2014, 902164. https://doi.org/10.1155/2014/902164

Zhao, X., Zhou, G., Wei, C., Li, X., 2009. Effects of temperature gradients on elastic modulus and compression strength of the saturated frozen clay. Procedia Earth Planet. Sci. 1, 420–424.

Zhou, G., Hu, K., Zhao, X., Wang, J., Liang, H., Lu, G., 2015. Laboratory investigation on tensile strength characteristics of warm frozen soils. Cold Reg. Sci. Technol. 113, 81–90. https://doi.org/https://doi.org/10.1016/j.coldregions.2015.02.003

Zhou, M.M., Meschke, G., 2013. A three-phase thermo-hydro-mechanical finite element model for freezing soils. Int. J. Numer. Anal. methods Geomech. 37, 3173–3193.

Zhou, Z., Ma, W., Zhang, S., Cai, C., Mu, Y., Li, G., 2018a. Damage evolution and recrystallization enhancement of frozen loess. Int. J. Damage Mech. 27, 1131–1155. https://doi.org/10.1177/1056789517731138

Zhou, Z., Ma, W., Zhang, S., Mu, Y., Li, G., 2018b. Effect of freeze-thaw cycles in mechanical behaviors of frozen loess. Cold Reg. Sci. Technol. 146, 9–18. https://doi.org/https://doi.org/10.1016/j.coldregions.2017.11.011